# Interruption of paracellular bile acid cycling after acetaminophen overdose ameliorates hepatotoxicity

Ahmed Ghallab, Reham Hassan, Ute Hofmann, Adrian Friebel, Zaynab Hobloss, Lisa Brackhagen, Brigitte Begher-Tibbe, Maiju Myllys, Joerg Reinders, Nina Overbeck, Selahaddin Sezgin, Sebastian Zühlke, Abdel-latif Seddek, Walaa Murad, Tim Brecklinghaus, Franziska Kappenberg, Jörg Rahnenführer, Daniela González, Christopher Goldring, Ian M. Copple, Rosemarie Marchan, Thomas Longerich, Mihael Vucur, Tom Luedde, Stephan Urban, Ali Canbay, Thomas Schreiter, Michael Trauner, Jephte Y. Akakpo, Mojtaba Olyaee, Steven C. Curry, Jan-Peter Sowa, Hartmut Jaeschke, Stefan Hoehme, Jan G. Hengstler

Table of contents

## Supplementary materials and methods

### Materials

Materials and resources are summarized in the Supplementary CTAT Table.

### Patients

*Phoenix patient:* A 19-year-old woman, body weight 69 kg, purchased a bottle of APAP/ *diphenhydramine* tablets, promptly ingested 86.5g APAP and 4.325g *diphenhydramine* and immediately sought care, arriving 70 minutes post-ingestion. Time of ingestion was confirmed by the receipt of drug purchase, and remaining pill counts were in keeping with history. The patient vomited and then received activated charcoal. Intravenous N-acetylcysteine (NAC) was commenced <2 hours post-ingestion and was continued at 7.25 mg/kg b.w./hour after 20 hours for a total NAC infusion time of 145 hours, because of unexpected progressive toxicity. APAP concentrations in blood were 562 mg/L (3.7 mM) and 333 mg/L (2.2 mM) at 1.7 and 4 hours post ingestion, respectively. Overall, the clinical course was characterized by hepatotoxicity and significant hemolysis from accompanying glucose-6-phosphate dehydrogenase deficiency. Renal function remained normal, and 260 hours post-ingestion clinical chemistry showed AST 35 U/L, ALT 714 U/L (falling), bilirubin 1.5 mg/dL, and hemoglobin 12.2 g/dL.

### Mice

Male 8–12-week-old C57BL6/N (Janvier Labs, France) or Oatp-deficient mice (Taconic Biosciences, USA; Cat. No. 10707-M; FVB.129P2-Del(Slco1b2-Slco1a5)1Ahs) and corresponding wild-type mice (Taconic Biosciences, USA; Cat. No. FVB-M) were used. The mice were housed under 12 h light/dark cycles at controlled ambient temperature of 25 °C with free access to water. The mice were fed ad libitum with Ssniff R/M-H, 10 mm standard diet (Ssniff, Soest, Germany) before starting the experiments. All experiments were approved by the local animal welfare committee (LANUV, North Rhine-Westphalia, Germany, application number: 84-02.04.2016.A279).

### Induction of acute liver injury by APAP

In order to induce acute liver injury by acetaminophen (APAP), a single dose of 300 mg/kg b.w. was intraperitoneally (i.p) injected in warm phosphate-buffered saline (PBS) [1-3]. The application volume was 30 ml/kg b.w. The mice were starved overnight prior to APAP application and were fed ad libitum afterwards.

**Glutathione depletion experiments**
GSH depletion was induced by combined administration of buthionine-sulfoximine (BSO) and diethyl maleate (DEM), as previously described [4]. Briefly, overnight-fasted mice were first treated with BSO (0.6 g/kg bw; i.p. dissolved in PBS pH 7.4; application volume 20 ml/kg); 30 minutes later, the mice were further treated with DEM (0.75 ml/kg bw; i.p.). Samples were collected time-dependently after DEM treatment.

**Induction of apoptosis**
As a positive control for apoptosis, mice were challenged with 700 mg/kg bw D-(+)-galactosamine hydrochloride (i.p. in PBS) and 100 mg/kg lipopolysaccharides from Escherichia coli O55:B5 (i.v. in PBS) for 6 hours, as previously described [5].

**Bile flow analysis**
The volume of bile outflow was measured in male C57Bl6/n mice by fixing a catheter in the extrahepatic common bile duct as previously described [6, 7]. Bile obtained in the first 40 minutes was discarded to allow stable flow rate. Bile flow rate was determined for 20 minutes before and up to 200 minutes after PBS, APAP, or BSO+DEM treatment. The results were normalized to the bodyweight.

**Intervention experiments**
In order to interrupt bile acid cycling observed after APAP intoxication the sinusoidal uptake transporters were blocked. For this purpose, male Oatp knockout and the corresponding wildtype FVB mice were used. The mice were fasted overnight prior to i.p application of 300 mg/kg b.w. APAP. Simultaneously with the APAP injection, the Oatp knockout mice additionally received an intravenous bolus injection of Myrcludex B (5 mg/kg b.w.). Blood as well as liver tissue samples were collected on day one after APAP injection to evaluate liver damage. Additionally, to investigate APAP metabolism, blood as well as liver tissue samples were collected before as well as at 30 minutes, 1, 2, and 4 hours after APAP administration.

**Intravital imaging**
Functional intravital imaging of mouse livers was done using an inverted two-photon microscope LSM MP7 (Zeiss, Germany) with an LD C-Apochromat 40x/ 1.1 water immersion objective, as previously described[6, 8-12]. The mice were anesthetised by an intraperitoneal cocktail injection of ketamine (100 mg/kg b.w.), xylazine (10 mg/kg b.w.),

acepromazine (1.7 mg/kg b.w.), and buprenorphine (0.08 mg/kg b.w.). Bolus tail vein injections of Hoechst 33258 (nucleus marker), TMRE (marker of lobular zonation and mitochondrial membrane potential), and propidium iodide (marker of cell death) were given immediately before mouse surgery and recording (Supplementary Table 1). To allow administration of further functional dyes/markers while recording, a mouse catheter (SAI-infusion, IL, USA) was fixed in the tail vein. The left liver lobe was exposed by performing a midline incision in the abdominal wall caudal to the sternum. The coronary ligament which connects the liver to the diaphragm was cut in order to minimize the influence of breathing. The exposed left liver lobe was placed onto a cover slip (0.17 mm-thick; Logitech, Glasgow, UK) fitted in a custom-made image platform, and was covered with a saline-soaked piece of gauze. Anaesthesia was maintained along the entire recording period using an isoflurane inhaler (0.5-1 %). The bile acid analogue CLF was administered via the tail vein catheter either as a bolus (1 mg/kg b.w.) or as continuous perfusion (1 mg/kg b.w. per hour), as indicated in the result section (Supplementary Table 1). Similarly, bolus tail vein injections of fluorescein-coupled dextran, 70 kDa, or CMFDA were administered while recording (Supplementary Table 1). To detect reactive oxygen species (ROS), the general oxidative stress indicator 2',7'-dichlorofluorescein diacetate ($H_2$DCFDA) was administered i.v. (0.5 mg/kg b.w.; dissolved in DMSO with an application volume of 1 ml/kg b.w.) 10 minutes prior to imaging. At least three mice were analysed for each of the experimental scenarios shown in the result section.

**Sample collection and processing**

Blood as well as liver tissue samples were collected from defined anatomical positions of anesthetized mice as described in [13-15]. The blood samples were collected from the portal vein (representing the liver inflow), the hepatic vein (representing the liver outflow), and the right heart chamber (representing the systemic blood) [13], in syringes coated with disodium ethylenediaminetetraacetic acid (EDTA). After centrifugation, plasma was isolated and stored at -80 ° C until used for the analysis of bile acida or liver enzymes. Following blood collection, the remaining blood was washed by transcardial perfusion with PBS. Subsequently, the liver was excised and two specimens of approximately 1 cm were collected from the left liver lobe; one specimen was fixed in 4% paraformaldehyde (PFA) for 2 days, and further processed and embedded in paraffin to be used for

histopathology and immunohistochemistry analyses; the other specimen was snap-frozen in liquid nitrogen to be used for MALDI-MSI analysis as well as for preparation of tissue slices for immunostaining and three-dimensional reconstructions[6, 14]. The remaining liver tissue was shock-frozen by freeze-clamping and milling in liquid nitrogen and was stored at -80° C until used for bile acid assay.

**Liver enzyme assay**

The alanine transaminase (ALT) and aspartate transaminase (AST) activity assays were performed using heart blood plasma with the Piccolo Xpress Clinical Chemistry Analyzer (Hitado, Germany).

**Bile acid assay**

Bile acid concentrations in plasma, bile, liver tissue and cells were determined by negative electrospray (ESI) liquid chromatography tandem mass spectrometry (LC-MS/MS) in multiple-reaction-monitoring (MRM) mode on an Agilent 6495B triple quadrupole mass spectrometer (Agilent, Germany) coupled to an Agilent Infinity II HPLC system as described previously[6, 16]. Briefly, frozen tissue samples were homogenized in methanol: water 1:1 (v/v) in a FastPrep® 24 homogenizer (MP Biomedicals, Santa Ana, USA) to a final concentration of 40 mg wet tissue/ml as described previously[17]. Cell lysates were prepared by ultrasonic extraction of cell pellets with methanol: water (1:1, v/v), or of cells cultured in collagen matrix with methanol. Aliquots of 5 µL of serum or diluted bile (1:100), 30 µl of tissue homogenate, or 25 µl of cell lysate were spiked with internal standard solution followed by protein precipitation with methanol and centrifugation. The supernatant was used for LC-MS/MS analysis. Protein was determined in tissue homogenates using bicinchoninic acid[18]. DNA quantification was performed using bisBenzimide (DNA quantitation kit, Merck, Darmstadt, Germany).

**MALDI-MSI of taurocholic acid, glutathione, and acetaminophen-glutathione**

MALDI-MSI analysis of taurocholic acid (TCA), GSH, and APAP-GSH were performed using TIMS TOF Flex as previously described [3, 6]. Sets of consecutively cut 5 µm-thick liver tissue sections from the left liver lobes were prepared for MALDI measurements as well as for Cyp2e1 immunostaining. Signals of the MALDI ion density images obtained from the MS measurements were superimposed onto adjacent sections stained by the pericentral zonation marker Cyp2e1. For MALDI analysis, the tissue sections were treated

with 2-mercaptobenzothiazole matrix using HTX TM –Sprayer, Model: TMSP M3 Rev. 19. For TCA analysis, the ion [M-H]-, m/z 514.2839 was tracked within a mass tolerance window of ± 50 ppm in the negative ion mode using the Scils Lab Version 2021c Pro [3]. Quantification of the TCA signal was performed by Scils software [19]. GSH and APAP-GSH were also tracked in the [M-H]-ion. APAP-GSH, with its m/z of 455,1276 was tracked within a mass tolerance of 30 ppm. GSH with its m/z of 306,0776 was tracked within a mass tolerance of 40 ppm.

**Determination of 4-hydroxy-nonenal-adducts**

Snap-frozen liver tissue samples were homogenized in 200 µL PBS supplemented with 0.5% Triton X-100 using 5 cycles (30 s ON/30 s OFF with glass beads) in a Bioruptor (Diagenode Inc., USA). After centrifugation at 21,000 × g for 5 minutes, the supernatant was stored at -80 °C until measurement. 4-hydroxy-nonenal-adducts were measured using the Lipid Peroxidation (4-HNE) Assay Kit (Abcam, UK) according to manufacturer´s instructions. Duplicate measurements were conducted for all samples using 50 µL of sample.

**Staining of fixed liver tissue**

Two-dimensional (2D) hematoxylin and eosin, immunohistochemistry, as well as TUNEL stainings were performed in 5 µm-thick paraformaldehyde (4%)-fixed paraffin-embedded liver tissue sections. The staining was done on the Discovery Ultra Automated Slide Preparation System (Roche, Germany), as previously described [20]. TUNEL staining was done using a commercially available kit (Promega, Germany). Antibodies used for immunostaining as well as their concentrations are given under Suppl. Table 2. Nuclei were visualized by counter-staining with Mayer’s hematoxylin. Whole slide scanning was performed using Axio Scan.Z1 (Zeiss, Germany). Three-dimensional (3D) co-staining of Cyp2e1 and CD13 (Suppl. Table 2) was done in 100 µm-thick liver tissue slices prepared using a cryostat microtome as previously described [14]. Z-stacks of approximately 60 µm-depth were acquired using a laser scanning microscope (Olympus), and 3D reconstruction was performed using Imaris software.

**GSH assay**

Concentrations of reduced as well as oxidized glutathione (GSH) in liver tissue homogenate and bile were measured by LC-MS/MS as previously described [2, 3]. The results in liver tissue were normalized to the wet weight of the liver tissue sample.

**Analysis of APAP, APAP metabolites and APAP adducts**

Concentrations of APAP, its glucuronide and sulfate metabolites, as well as its glutathione, cysteine, and N-acetylcysteine adducts were measured in plasma separated from hear blood using HPLC-HR-MS, as previously described [1-3].

**Isolation and cultivation of mouse hepatocytes**

Hepatocytes were isolated from 8–10-week-old male C57BL6/N mice and were cultivated in collagen sandwich using a standard protocol [21] (main Figure 4A). Briefly, following isolation and counting, the cells were seeded in 24-well plates, pre-coated with a first layer of collagen (250 µg/ml rat tail collagen I), at a density of 400.000 cells/well. The cells were allowed to attach for 3 hours and then a second layer of collagen was added. One hour later, the cells were supplemented with fresh William's E medium containing various concentrations of mouse bile acids (0, 1, 10, 100, 316, 1000, and 3116 µM) and APAP (0, 1, and 4 mM). After incubation for 21 hours, cytotoxicity was determined using the CellTiter-Blue Cell Viability Assay, according to the manufacturer instructions (Promega).

For quantification of intracellular concentrations of bile acids, mouse hepatocytes were isolated, and seeded in the same way. After addition of the second layer of collagen, the cells were incubated with various concentrations of mouse bile acids (0, 10, 100, and 1000 µM) for 2 hours. After washing steps, the cells were harvested, shock-frozen in liquid nitrogen, and stored at -80° C until used for bile acid quantification.

To determine the intracellular concentrations of bile acids after APAP intoxication, male C57BL6/N mice were treated with APAP (300 mg/kg) or PBS. Two hours later, the mice were anaesthetised and biopsies of approximately 20 mg were taken, and the livers were immediately perfused, and hepatocytes were isolated. After cell counting, 800.000 cells were shock-frozen and stored at -80° C until used for quantification of bile acids.

## Image analysis

All segmentations were generated with one of the interactive image segmentation toolkits ilastik [22] (version 1.3.3post1), TiQuant [23] (version 2.0) or QuPath [24] (version 0.2.3), as indicated below. Pre-processing as well as post-processing and quantification was done using Jupyter Notebook [25] with Python using several image processing modules: SimpleITK [26], scikit-image [27], opencv[28], PlantCV [29] and StackReg [30].

## Analysis of CLF-associated fluorescence in sinusoids, hepatocytes, and bile canaliculi in intravital two-photon time series

Videos from control and APAP-treated mice were flattened by z-projection using median as operator for the Hoechst (blue) and TMRE (red) channel, maximum intensity for the CLF (green) channel of the control dataset and standard deviation for the CLF channel of the APAP dataset. The resulting z-projections of the individual channels were reassembled into 2D RGB images. The control and APAP 2D images were subsequently segmented using ilastik's pixel classification workflow. For both images separate classifiers were interactively trained using all available features with all pre-defined sigmas to differentiate sinusoid, hepatocyte and bile canaliculi compartments. Similarly, classifiers were trained for a partitioning into peri-central and peri-portal zones, with the difference that sigmas <1 were deselected. Zonation masks were post-processed with a morphological closing and opening operation to smooth up the zonal border. Finally, mean and standard deviation of CLF intensity per compartment and zone in each frame were measured.

## Intravital time series after APAP: Analysis of CLF intensity changes per compartment, bile canaliculi diameter and quantification of blebbing-events

This time series exhibits considerable tissue movement preventing direct application of a z-projection. Therefore, the dataset was first registered with StackReg [31] using an affine transformation, correcting for translation, rotation, scaling and shearing. The registration was done in the Hoechst (blue) channel, since the staining was consistent over time. Due to rapid intensity fluctuations between consecutive frames a moving average of ten frames was used to register to the mean of the first ten frames. The resulting transformation was applied to all three-color channels yielding a stabilized time series.

The TMRE (red) channel was normalized using Fiji's [30] automated brightness and contrast adaptation and subsequently the maximum-intensity z-projection was calculated for all three color channels for frames 4100 to 4200. The pixel classification workflow of ilastik was used to train two classifiers differentiating blebs and bile canaliculi, as well as cells and sinusoidal lumina, respectively. The zonation mask was annotated manually. During post-processing, the hepatocyte segmentation was masked with the bile segmentation to prevent overlap between compartments. Mean and standard deviation of CLF intensity per cell and bile canaliculi compartment and zone in each frame was measured. Notably, blebs were not considered separately and instead were attributed to the hepatocyte compartment.

For measuring the number and areas of blebs over time a fixed CLF intensity threshold (40) was assumed, above which a pixel in the previously segmented bleb compartment (2D) was considered active. For each bleb in each frame the number of active pixels was measured, and if more than ten percent of a bleb's pixels were active, the bleb was considered active.

**Intravital 2D tile scans after APAP intoxication: Analysis of bile canaliculi diameter in relation to zonation**

For segmentation of bile canaliculi ilastik's pixel classification workflow was employed. The classifier was trained from sparse annotations of one of the images using all features and default sigmas. In a first post-processing step the original images and corresponding binary segmentations were upscaled by a factor of three to increase the accuracy of the subsequent bile canaliculi diameter measurement. Morphological closing was used to close small gaps in the binary mask. Connected bile canaliculi objects were extracted and very small objects (<10 pixels) as well as very large objects (>3k pixels) were excluded from the following measurement, as they were found to be largely false positives (either small noise patches or large blebs). For the remaining objects, skeletons were computed, which are 1-pixel-wide, topology-preserving lines following the medical axis of an object, using Lee's method [32]. The resulting skeletons were pruned using PlantCV, cutting offside-branches shorter than 30 pixels, ensuring that small protuberances at the canalicular surface did not introduce artificial side branches. In order to be able to use the

TMRE signal as a measure for zonation it was locally smoothed using a mean filter with a rectangular kernel with side-length 20 pixel. The intensity range was then subdivided into 10 equally sized intervals. Finally, for every skeleton pixel its distance to the closest pixel not segmented as bile canaliculus was calculated which equals the radius, together with its smoothed TMRE intensity and interval.

**Bright-field whole slide scans: Analysis of the bile canalicular diameter in relation to zonation**

Tissue, pericentral regions and bile canaliculi were segmented in this set of bright-field scans with QuPath that allows to work with (tiled) pyramid image formats. A threshold on the green channel was used for tissue segmentation at a pixel resolution of 0.4 µm. The neural network classifier was interactively trained at a resolution of 1.77 µm to segment the pericentral regions, and at 0.22 µm to segment the bile canaliculi. During post-processing, which was performed at a pixel-resolution of 0.22 µm, the tissue mask was eroded to remove a 30 µm-wide margin and the bile canaliculi segmentation was divided into a pericentral and a periportal part based on the pericentral marker Cyp2e1 that was visualized by immunostaining. Closing was applied to the bile canaliculi segmentation with a kernel size of 4 to close small holes in the mask. Analogous to the procedure applied to the intravital tile scans bile canaliculi skeletons were calculated and radii measured at every skeleton pixel. Finally, the top 0.2% skeleton pixels in regard to diameter per pericentral and -portal regions were excluded from analysis, as they were considered to represent the few misclassifications of wide collagenous objects.

For the BSO/DEM experiment, random forest classifiers were interactively trained at a resolution of 0.44 µm for tissue segmentation, at a resolution of 3.54 µm to segment the pericentral regions, and at 0.22 µm for bile canaliculi segmentation. During post-processing, performed at a pixel-resolution of 0.22 µm, the bile canaliculi segmentation was divided into a pericentral and a periportal part based on the segmentation of pericentral regions and closing was applied to it with kernel size 4. Bile canaliculi skeletons were calculated, and radii measured at every skeleton pixel. Finally, the top 1% of skeleton pixels regarding diameter per image were excluded from analysis, as they were considered to represent the few misclassifications of wide collagenous objects.

## Quantification of dead cell areas in whole slide scans of fixed liver tissue

For segmentation of tissue and dead cell areas, TiQuant was used. A random forest classifier was interactively trained to learn corresponding superpixel class memberships at a resolution of 1.77 µm using R/G/B histograms and gradient magnitude features. The resulting dead cell regions as fractions of total tissue were computed based on the resulting masks without further post-processing.

## Statistical analysis

Data were analyzed using Prism software (GraphPad Prism 7.05 Software, Inc., La Jolla, CA). Statistical significance between experimental groups was analyzed using Dunnett's/ Tukey's/ Sidak's multiple comparisons test, or unpaired t test, as indicated in the figure legends. Concentration-cytotoxicity relationships were described by a three-parameter log-logistic model, where in comparison to a four-parametric log-logistic model as described [33], the lower limit (i.e. parameter c) was fixed to take a value of 0. The normalization in the re-fit procedure was conducted with respect to the upper asymptote of the curve corresponding to 0 mM APAP. Relative EC values were calculated as the concentration where the curve attains the corresponding proportion of the upper asymptote, (e.g. EC10 corresponds to a response of 90% of the upper asymptote), and confidence intervals were calculated as described [33]. The curve fitting was conducted using the R-package drc, version 3.0-1 [34].

## Supplementary video legends

**Video S1:** Two-photon imaging of a mouse liver beginning 85 minutes after APAP overdose (300 mg/kg). Corresponding to the stills in Fig. 2C.

**Video S2:** Intravital imaging of transport of the green-fluorescent bile acid analogue CLF after intravenous bolus injection in healthy and in APAP-intoxicated (85 minutes) mice. Corresponding to Fig. 3A.

**Video S3:** Intravital imaging of the livers of control and APAP-intoxicated (90 minutes) mice after tail vein injection of fluorescein-coupled Dextran 70 kDa (green). Corresponding to Fig. 3H.

**Video S4:** Intravital imaging of the livers of control and APAP-intoxicated (80 minutes) mice after bolus tail vein injection of CMFDA. Corresponding to Fig. 3H.

**Video S5:** Intravital imaging of a mouse liver starting at 3 hours after BSO/DEM injection. Corresponding to Fig. 5E.

## Supplementary figures

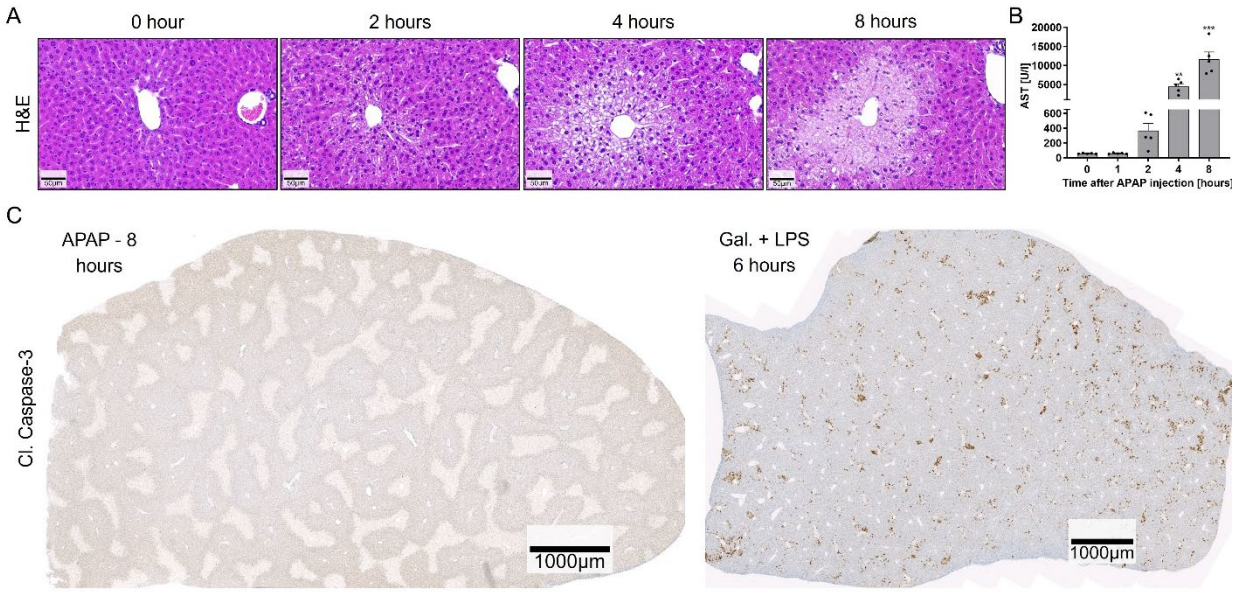


**Fig. S1. Induction of pericentral liver injury by injection of a high dose of acetaminophen (APAP, 300 mg/kg b.w.). A.** Hematoxylin and eosin (H&E) staining before as well as at different time periods after APAP injection showing pericentral hepatocyte damage at 4 and 8 hours after APAP injection. Scale bars: 50 µm. **B.** Aspartate transaminase (AST) activity in blood plasma showing significant elevation at 4 and 8 hours after APAP injection. The data are presented as mean± SE and considered significant at $p<0.01$ (**) and $p<0.01$ (***) (one-way ANOVA, Dunnett's multiple comparisons test). **C.** Whole slide scans of liver tissue sections treated with APAP or galactosamine plus LPS after immunostaining using antibodies against cleaved caspase-3. This suppl. Figure corresponds to the main figure 1E, F.

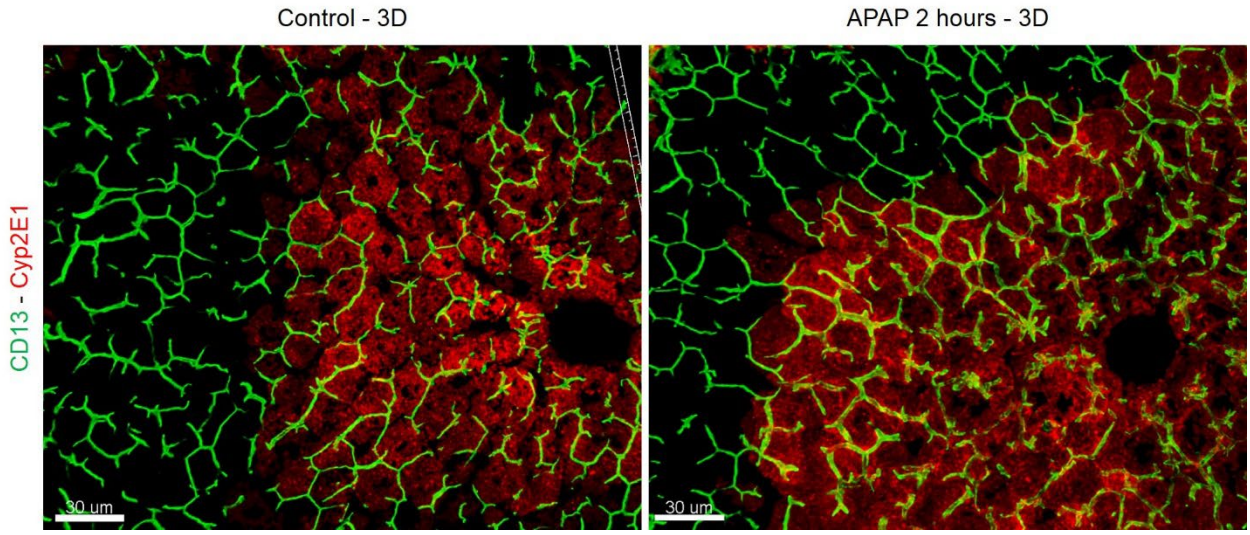


**Fig. S2. Massive dilatation of bile canaliculi in the pericentral compartment of the liver lobule after acetaminophen (APAP) intoxication.** Three-dimensional reconstruction of CD13 (green) and Cyp2e1 (red) immunostaining before as well as at 2 hours after injection of 300 mg/kg b.w. APAP. The images show dilatation of bile canaliculi in the Cyp2e1 positive hepatocytes after APAP intoxication. Scale bars: 30 µm. The images correspond to the main figure 2F, G.

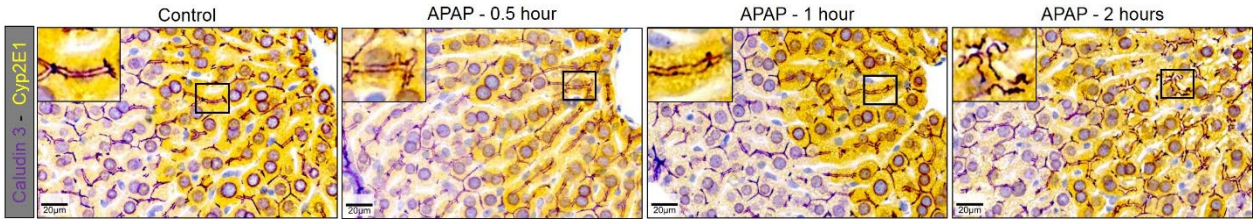


**Fig. S3. Compromised tight-junction morphology after intoxication with acetaminophen (APAP, 300 mg/kg b.w.).** Co-staining of liver tissue sections collected at different time intervals after APAP injection using antibodies against Cyp2e1 (yellow) and Claudin3 (purple) showing altered tight-junction morphology after APAP intoxication particularly at 2 hours characterized by massive dilatation between the two strands and irregular staining pattern. Scale bars: 20 µm. The images correspond to the main figure 3G.

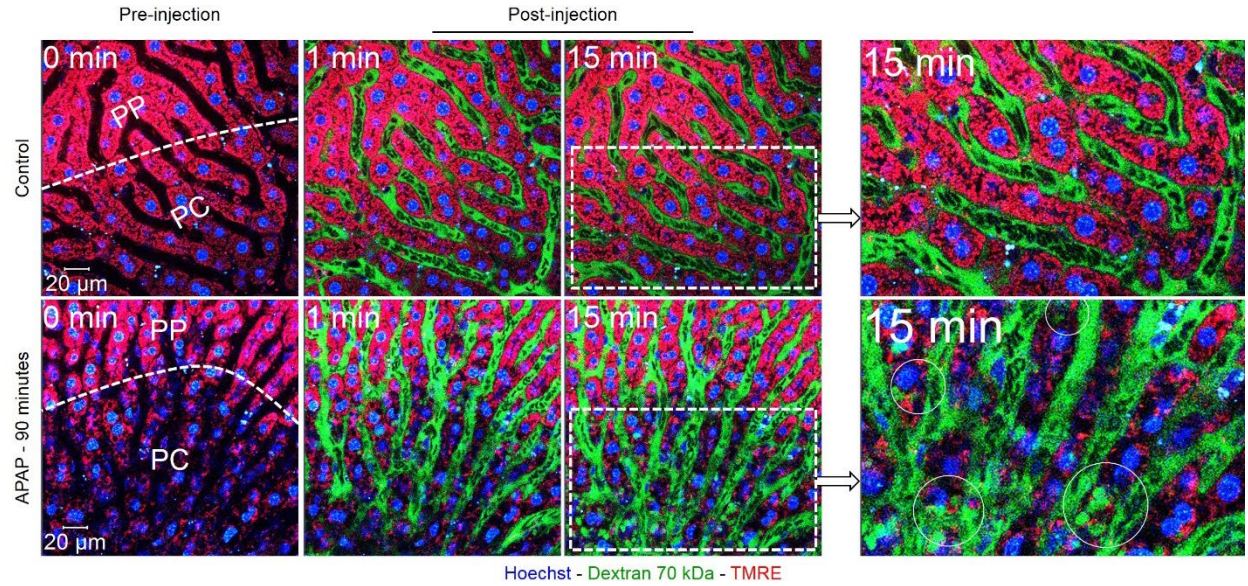


**Fig. S4. Leakiness of the blood-bile barrier after intoxication with acetaminophen (APAP, 300 mg/kg b.w.).** Stills from intravital videos of control as well as APAP- (90 minutes) treated mice before as well as after bolus intravenous injection of fluorescein-coupled dextran (70 kDa). In the control mouse dextran appeared in the blood sinusoids post-injection and never passed to the bile canaliculi within the recorded period. In contrast, after APAP intoxication dextran-associated green fluorescence also occurred in bile canaliculi of pericentral hepatocytes. Green: fluorescein-coupled dextran; red: TMRE; blue: Hoechst. The images correspond to the main Fig. 3H and Suppl. Videos 3A-C. PC: pericentral; PP: periportal; scale bars: 20 µm.

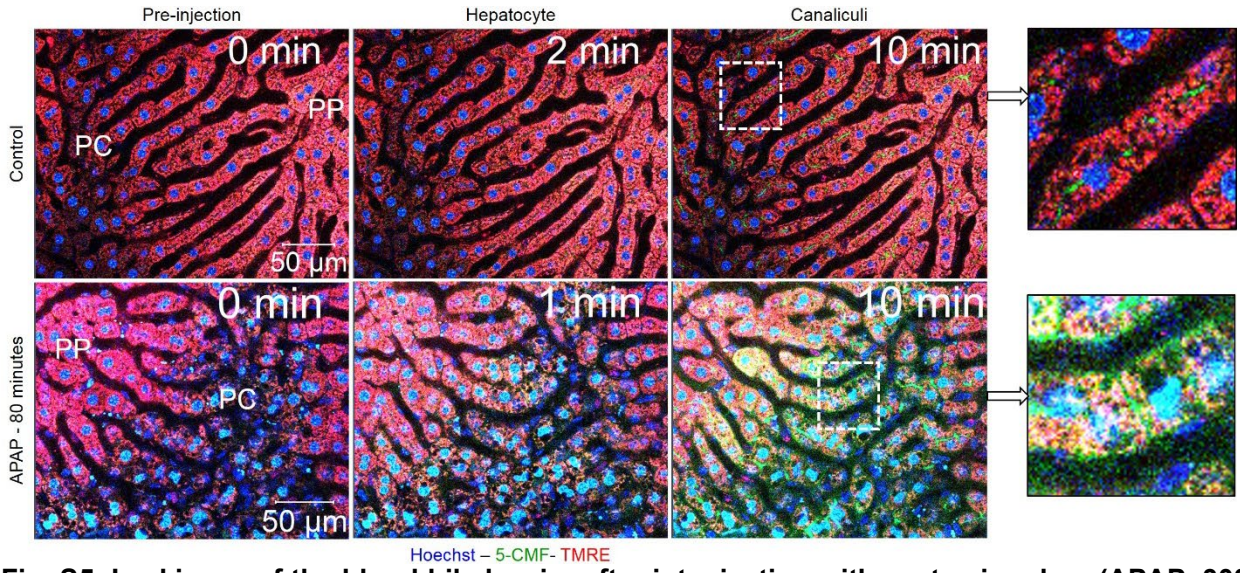


**Fig. S5. Leakiness of the blood-bile barrier after intoxication with acetaminophen (APAP, 300 mg/kg b.w.).** Stills from intravital videos of control as well as APAP- (80 minutes) treated mice before as well as after bolus intravenous injection of the tracer dye CMFDA. In the control mouse injection of CMFDA lead to green fluorescence in the hepatocyte cytoplasm followed by secretion to bile canaliculi; almost no green fluorescence could be detected in the blood sinusoids. In contrast, after APAP intoxication green fluorescence occurred also at the interface of pericentral hepatocytes and blood sinusoids. Green: 5-CMF; red: TMRE; blue: Hoechst. The images correspond to the main Fig. 3I and Suppl. Videos 4A-C. PC: pericentral; PP: periportal; scale bars: 50 µm.

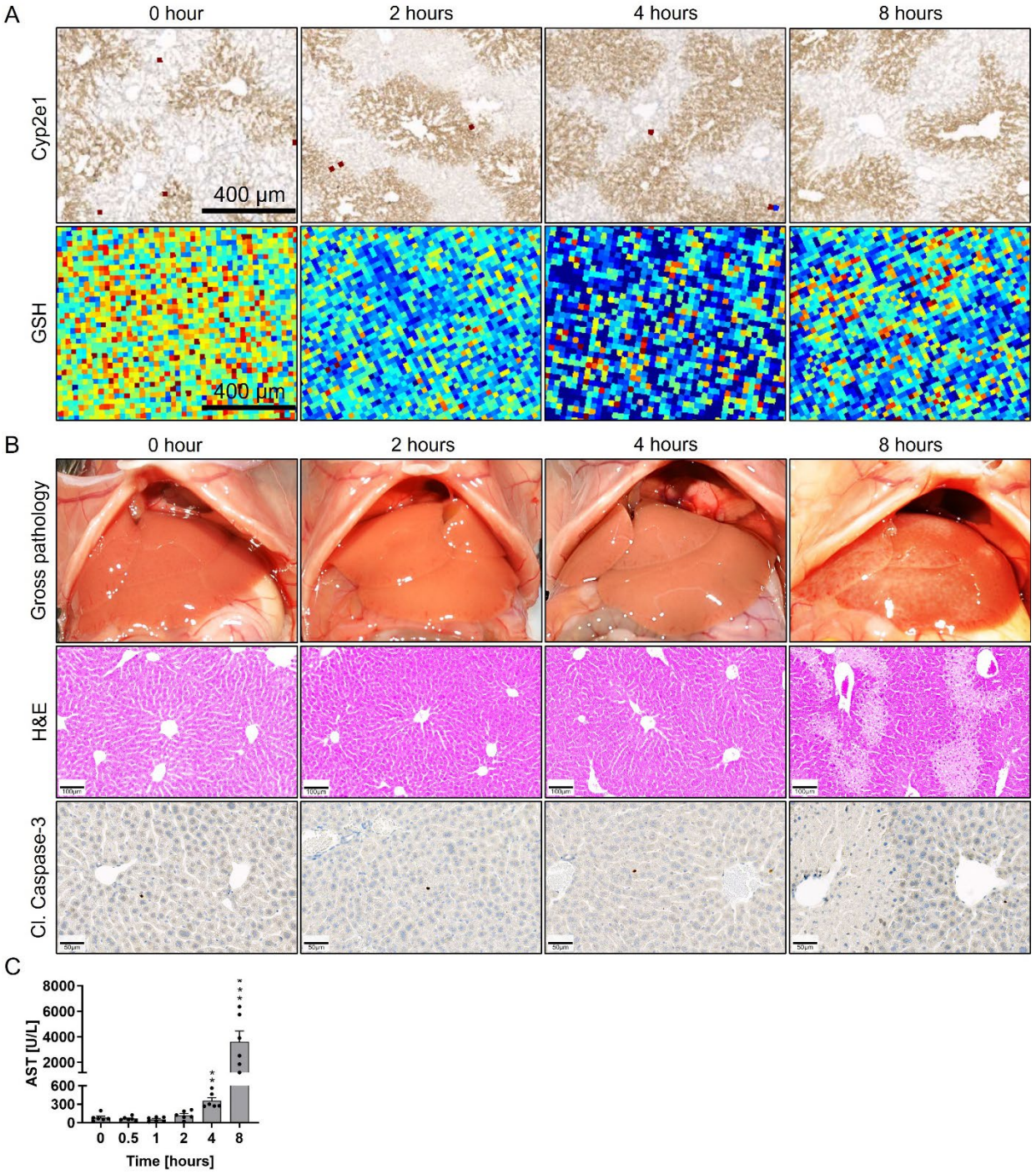


**Fig. S6.** Glutathione (GSH) depletion and liver damage after BSO plus DEM treatment. **A.** MALDI-MSI imaging of GSH before (0 hour) and at different time intervals after BSO plus DEM treatment; the images show homogeneous depletion in the Cyp2e1 positive and negative hepatocytes. **B.** Gross pathology, histopathology and cleaved caspase-3 staining before (0 hour) and at different time intervals after BSO plus DEM treatment. **C.** Aspartate transaminase (AST) activity in the blood before (0 hour) and at different time intervals after BSO plus DEM treatment.

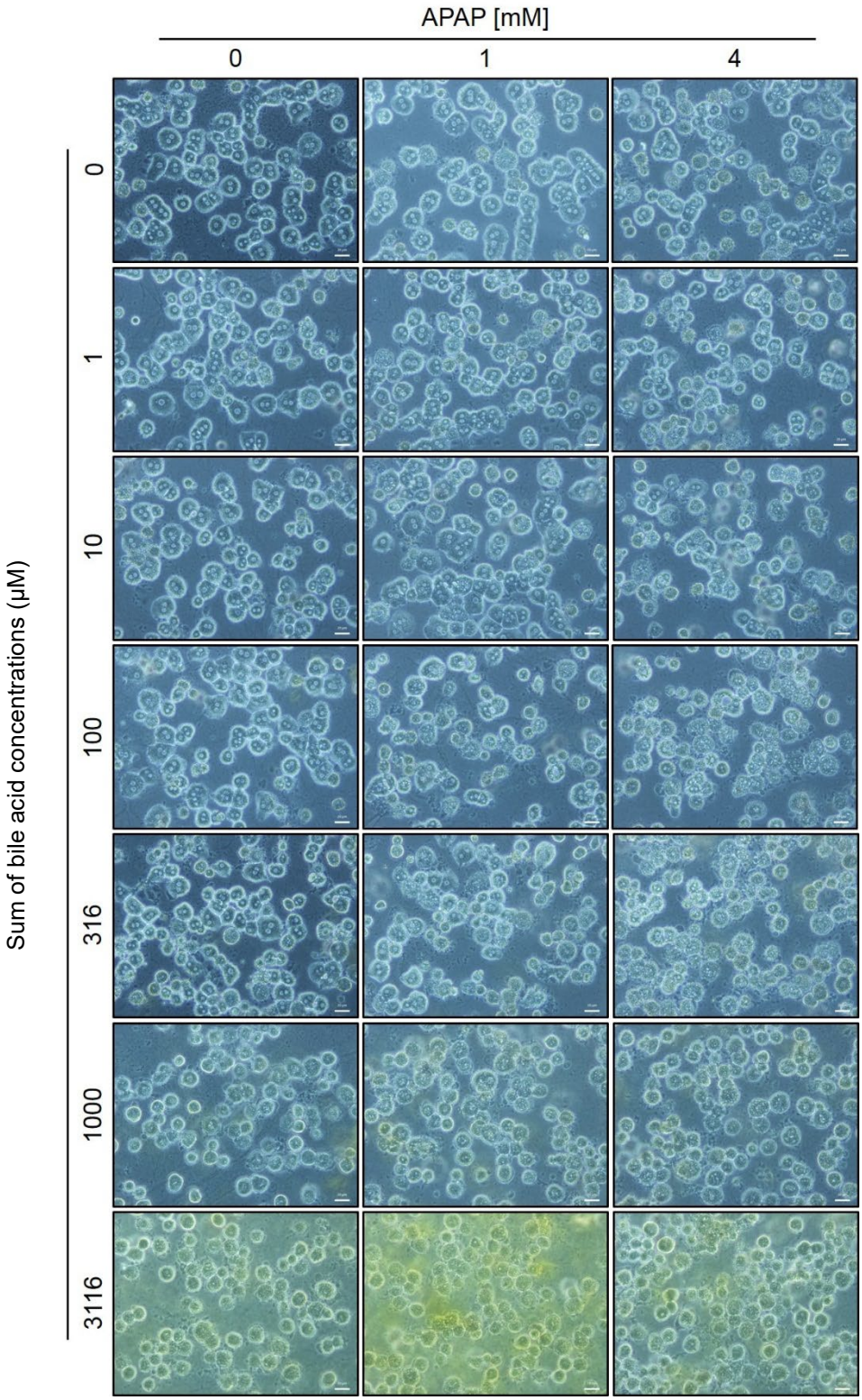


**Fig. S7. Concentration-dependent cytotoxicity of bile acids in cultivated mouse hepatocytes.** Phase contrast images of collagen sandwich culture of mouse hepatocytes 24 hours after incubation with various sum of bile acid concentrations showing concentration-dependent cytotoxicity. The images correspond to the main figure 4. Scale bars: 20 µm.

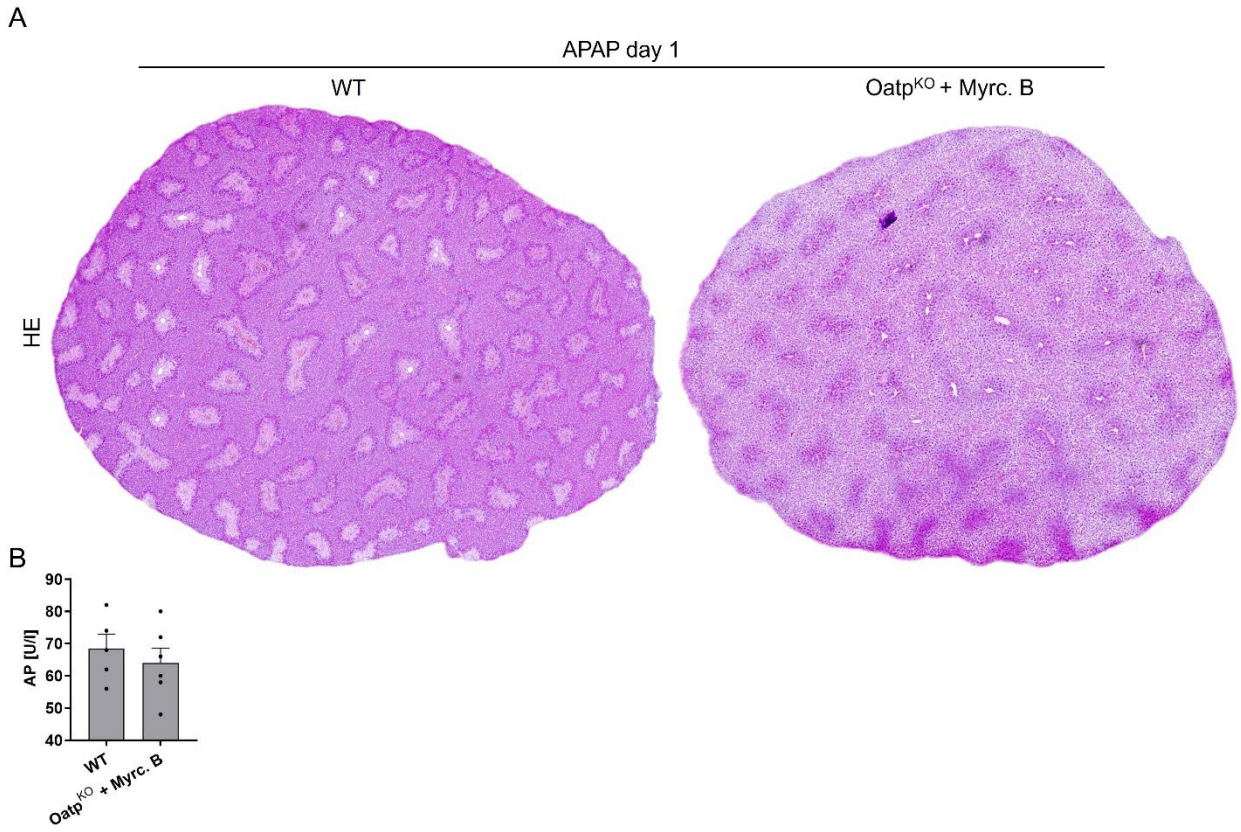


**Fig. S8. Blocking the sinusoidal uptake transporters of bile acids provides protection against acetaminophen (APAP) hepatotoxicity. A.** Whole slide scans of hematoxylin and eosin-stained liver tissue sections collected 24 hours after injection of 300 mg/kg b.w. APAP into wild-type (WT) or Oatp-deficient Myrcludex B-treated ($Oatp^{KO}$ + Myrcl. B) mice. The images show the typical APAP-induced pericentral liver damage in the WT but not in the $Oatp^{KO}$ + Myrcl. B mice. The images correspond to the main fig. 5 B, C. **B.** Alkaline phosphatase activity in the blood of wild-type (WT) and Oatp-deficient Myrcludex B-treated ($Oatp^{KO}$ + Myrcl. B) mice on day one after APAP administration.


**Fig. S9.** Whole slide scans showing similar Cyp2e1 expression in wild-type (WT) and Oatp-deficient mice. The images correspond to the main Fig. 5 E.

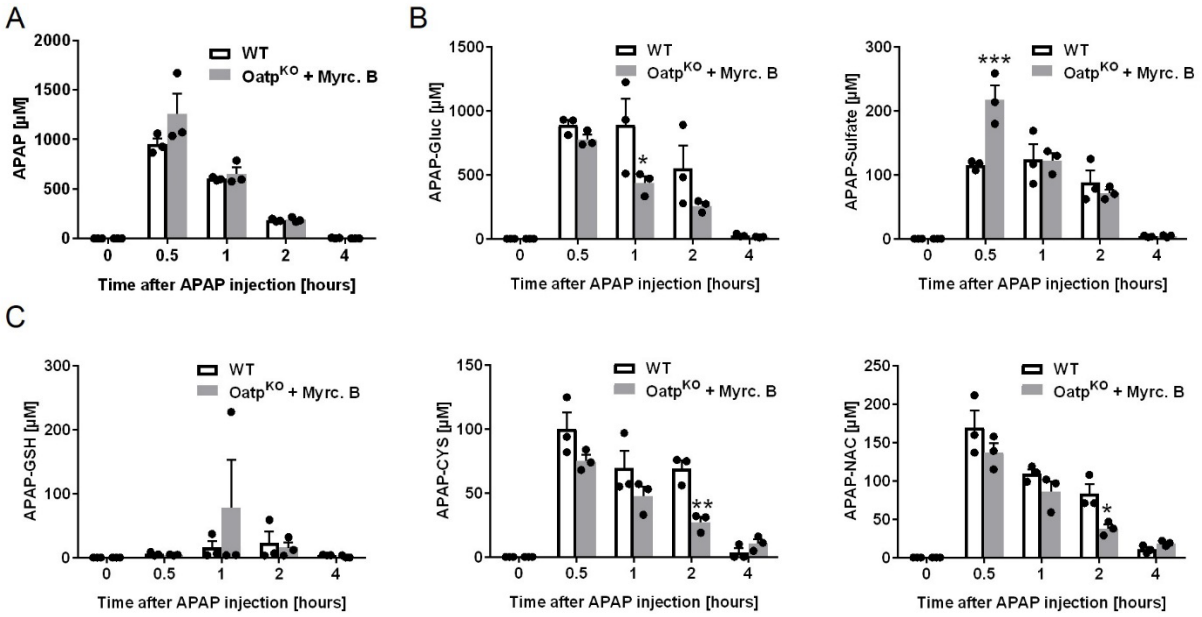


**Fig. S10. No systemic alteration in acetaminophen (APAP) clearance, metabolism or adduct formation after blocking the sinusoidal uptake transporters of bile acids.** Time-course of APAP, its glucuronide and sulfate metabolites, as well as its glutathione, cysteine, and N-acetylcysteine adducts after intraperitoneal injection of 300 mg/kg b.w. APAP into wild-type (WT) or Oatp-deficient Myrcludex B-treated (Oatp$^{KO}$ + Myrcl. B) mice showing no systemic difference between the two groups. The images correspond to the main fig. 5. The data are presented as mean± SE and considered significant at $p<0.05$ (*), $p<0.01$ (**), and $p<0.001$ (***), (two-way ANOVA, Sidak's multiple comparisons test).

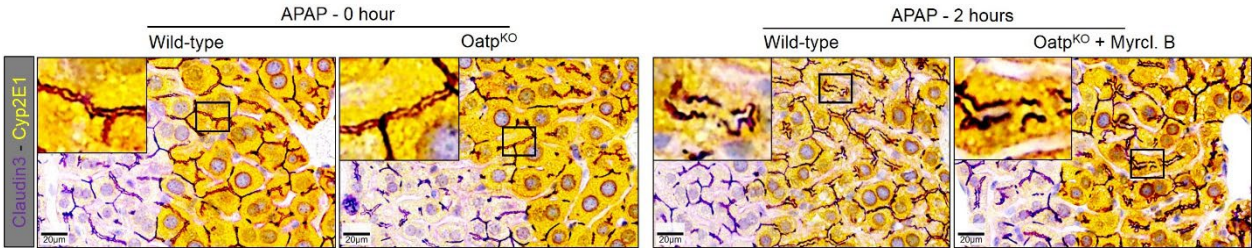


**Fig. S11. Similar alteration of the tight-junction morphology after acetaminophen (APAP) intoxication in** in wild-type (WT) and Oatp-deficient Myrcludex B-treated mice. The images correspond to the main fig. 5 G. Yellow: Cyp2e1; purple: Caludin3; scale bars: 20 µm.

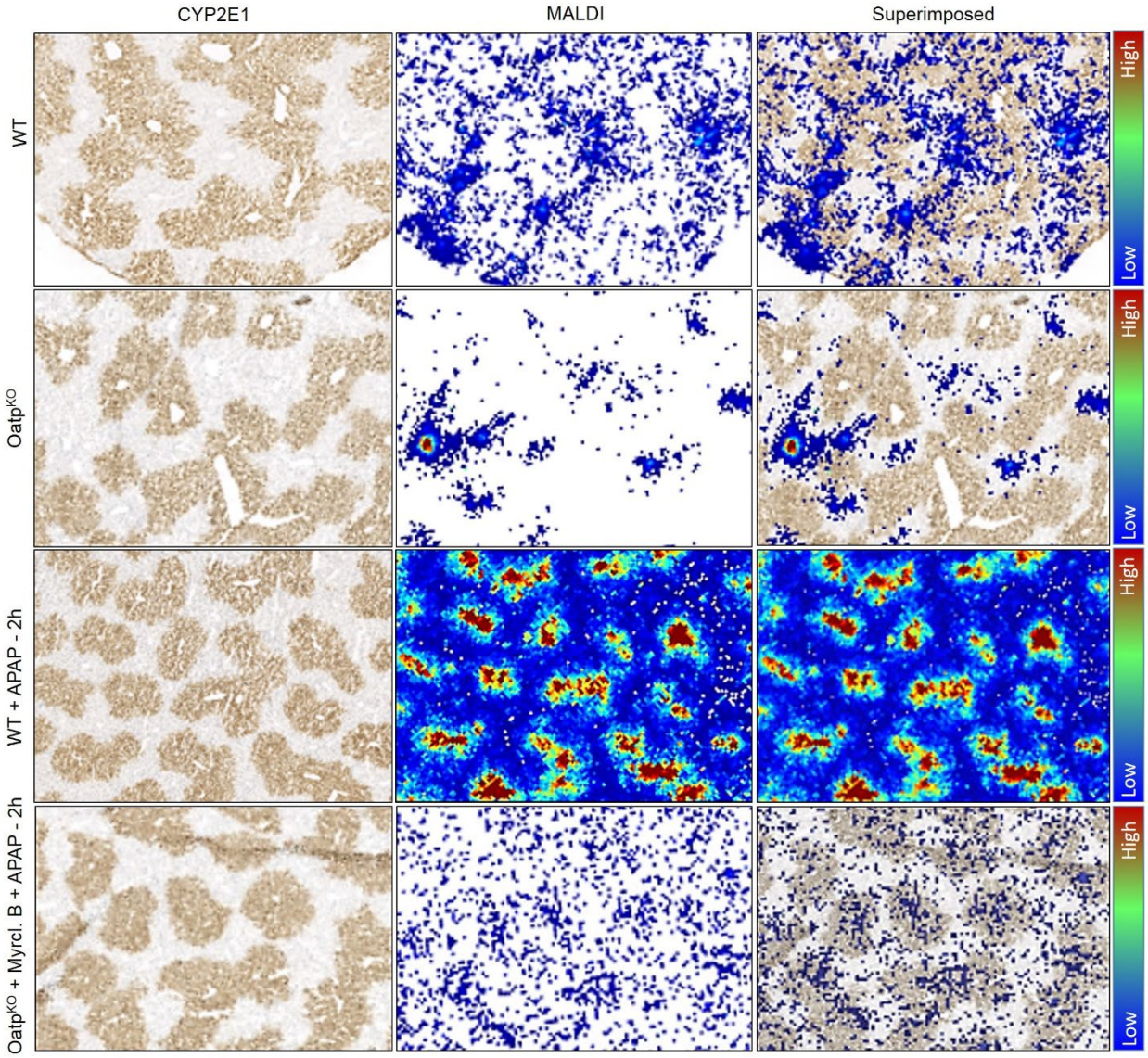


**Fig. S12. Blocking the sinusoidal uptake transporters strikingly reduced bile acid accumulation in the liver tissue after acetaminophen (APAP) intoxication.** Individual Cyp2e1 images, MALDI-MSI signal of taurocholic acid (TCA) or superimposed images prepared from serially cut liver tissue sections of wild-type (WT) and Oatp-deficient Myrcludex B-treated mice before and 2 hours after APAP injection (300 mg/kg b.w.). The images show massive accumulation of TCA in WT mice after APAP intoxication, particularly in the Cyp2e1 positive hepatocytes. In contrast, Oatp-deficient Myrcludex B-treated mice show only very little accumulation of TCA in the liver tissue after APAP injection. The images correspond to the main fig. 5I.

## Supplementary tables

**Table S1.** Fluorescent markers and functional dyes used in the study.

| Fluorescent marker/ reporter | Marker for | Dose [mg/kg] | Vehicle | Two-photon excitation range (nm) |
|---|---|---|---|---|
| Hoechst 33258 | Nuclei | 5 | PBS | 700-800 |
| TMRE | Lobular zonation; mitochondrial membrane potential | 0.96 | Methanol: PBS (1:1) | 740-820 |
| Propidium iodide | Membrane integrity/cell death | 2.67 | PBS | 720-800 |
| Cholyl-lysyl-fluorescein (CLF) | Bile acid analogue | 1 | PBS | 740-820 |
| Fluorescein-coupled dextran 70 kDa | Membrane integrity | 2 | PBS | 740-820 |
| 5-Chloromethylfluorescein diacetate (CMFDA) | Green-fluorescent tracer dye | 0.5 | methanol: PBS (1:10) | 740-820 |
| 2',7'-Dichlorofluorescein diacetate | Oxidative stress | 0.5 | DMSO | 950 |

**Table S2.** Antibodies used for immunohistochemistry.

| Target | Dimensions [D] | Primary antibodies | | Secondary antibodies | |
|---|---|---|---|---|---|
| | | Antibody | Dilution | Antibody | Dilution |
| Cyp2e1 | 2D | Anti-Cyp2e1 antibody, rabbit | 1:100 | Ultra-Map anti rabbit HRP | Automatic Discovery Ready to use |
| | 3D | Anti-Cyp2e1 antibody, rabbit | 1:50 | CyTM3-conjugated AffiniPure; F (ab') 2 fragment donkey anti-rabbit | 1:200 |
| Bile canaliculi | 2D | Recombinant anti-CD13 antibody, rabbit | 1:16000 | Ultra-Map anti rabbit HRP | Automatic Discovery Ready to use |
| | 3D | Anti-mouse CD13, rat | 1:100 | Alexa Fluor® 488 AffiniPure $F(ab')_2$ Fragment Donkey Anti-Rat IgG (H+L) | 1:200 |
| Tight junctions | 2D | Anti-ZO-1 polyclonal antibody, rabbit | 1:200 | Ultra-Map anti rabbit HRP | Automatic Discovery Ready to use |
| | | Anti-Claudin 3 polyclonal antibody, rabbit | 1:100 | Ultra-Map anti rabbit HRP | Automatic Discovery Ready to use |
| Apoptosis | 2D | Anti- cl. Caspase 3, rabbit | 100 | Ultra-Map anti rabbit HRP | Automatic Discovery Ready to use |

**Table S3.** Human patient data.

| Patient No. | Age [years] | Sex | AST [U/L] | ALT [U/L] | Sum of bile acid concentrations [µmol/L] |
|---|---|---|---|---|---|
| 1 | 39 | Male | 44 | 44 | 2 |
| 2 | 25 | Female | 224 | 20 | 275 |
| 3 | 62 | Female | 146 | 76 | 429 |
| 4 | 20 | Female | 140 | 902 | 316 |
| 5 | 40 | Female | 4148 | 1486 | 500 |
| 6 | 59 | Male | 3408 | 4904 | 6 |
| 7 | 28 | Male | 1924 | 1488 | 23 |
| 8 | 31 | Female | 2978 | 1330 | 13 |
| 9 | 22 | Female | 70 | 556 | 10 |
| 10 | 34 | Male | 2624 | 1164 | 2 |

## Supplementary references

### Author names in bold designate shared co-first authorship


[1] **Schneider KM, Elfers C**, Ghallab A, Schneider CV, Galvez EJC, Mohs A, et al. Intestinal Dysbiosis Amplifies Acetaminophen-Induced Acute Liver Injury. Cell Mol Gastroenterol Hepatol 2021;11:909-933.

[2] Schuran FA, Lommetz C, Steudter A, Ghallab A, Wieschendorf B, Schwinge D, et al. Aryl Hydrocarbon Receptor Activity in Hepatocytes Sensitizes to Hyperacute Acetaminophen-Induced Hepatotoxicity in Mice. Cell Mol Gastroenterol Hepatol 2021;11:371-388.

[3] Sezgin S, Hassan R, Zuhlke S, Kuepfer L, Hengstler JG, Spiteller M, et al. Spatio-temporal visualization of the distribution of acetaminophen as well as its metabolites and adducts in mouse livers by MALDI MSI. Arch Toxicol 2018;92:2963-2977.

[4] Monroe DH, Eaton DL. Effects of modulation of hepatic glutathione on biotransformation and covalent binding of aflatoxin B1 to DNA in the mouse. Toxicology and Applied Pharmacology 1988;94:118-127.

[5] Gujral JS, Knight TR, Farhood A, Bajt ML, Jaeschke H. Mode of cell death after acetaminophen overdose in mice: apoptosis or oncotic necrosis? Toxicol Sci 2002;67:322-328.

[6] Ghallab A, Hofmann U, Sezgin S, Vartak N, Hassan R, Zaza A, et al. Bile Microinfarcts in Cholestasis Are Initiated by Rupture of the Apical Hepatocyte Membrane and Cause Shunting of Bile to Sinusoidal Blood. Hepatology 2019;69:666-683.

[7] **Schneider KM, Candels LS,** Hov JR, Myllys M, Hassan R, Schneider CV, et al. Gut microbiota depletion exacerbates cholestatic liver injury via loss of FXR signalling. Nat Metab 2021;3:1228-1241.

[8] **Reif R, Ghallab A**, Beattie L, Gunther G, Kuepfer L, Kaye PM, et al. In vivo imaging of systemic transport and elimination of xenobiotics and endogenous molecules in mice. Arch Toxicol 2017;91:1335-1352.

[9] Koeppert S, Ghallab A, Peglow S, Winkler CF, Graeber S, Büscher A, et al. Live Imaging of Calciprotein Particle Clearance and Receptor Mediated Uptake: Role of Calciprotein Monomers. Frontiers in Cell and Developmental Biology 2021;9:1011.

[10] Koppert S, Buscher A, Babler A, Ghallab A, Buhl EM, Latz E, et al. Cellular Clearance and Biological Activity of Calciprotein Particles Depend on Their Maturation State and Crystallinity. Front Immunol 2018;9:1991.

[11] Vartak N, Guenther G, Joly F, Damle-Vartak A, Wibbelt G, Fickel J, et al. Intravital Dynamic and Correlative Imaging of Mouse Livers Reveals Diffusion-Dominated Canalicular and Flow-Augmented Ductular Bile Flux. Hepatology 2021;73:1531-1550.

[12] Ghallab A, Hassan R, Myllys M, Albrecht W, Friebel A, Hoehme S, et al. Subcellular spatio-temporal intravital kinetics of aflatoxin B1 and ochratoxin A in liver and kidney. Arch Toxicol 2021;95:2163-2177.

[13] Ghallab A, Celliere G, Henkel SG, Driesch D, Hoehme S, Hofmann U, et al. Model-guided identification of a therapeutic strategy to reduce hyperammonemia in liver diseases. J Hepatol 2016;64:860-871.

[14] Ghallab A, Myllys M, Holland CH, Zaza A, Murad W, Hassan R, et al. Influence of Liver Fibrosis on Lobular Zonation. Cells 2019;8.

[15] Schenk A, Ghallab A, Hofmann U, Hassan R, Schwarz M, Schuppert A, et al. Physiologically-based modelling in mice suggests an aggravated loss of clearance capacity after toxic liver damage. Sci Rep 2017;7:6224.

[16] Kube I, Tardio LB, Hofmann U, Ghallab A, Hengstler JG, Fuhrer D, et al. Hypothyroidism Increases Cholesterol Gallstone Prevalence in Mice by Elevated Hydrophobicity of Primary Bile Acids. Thyroid 2021.
[17] Leuthold P, Schaeffeler E, Winter S, Buttner F, Hofmann U, Murdter TE, et al. Comprehensive Metabolomic and Lipidomic Profiling of Human Kidney Tissue: A Platform Comparison. J Proteome Res 2017;16:933-944.
[18] Smith PK, Krohn RI, Hermanson GT, Mallia AK, Gartner FH, Provenzano MD, et al. Measurement of protein using bicinchoninic acid. Analytical biochemistry 1985;150:76-85.
[19] Robichaud G, Garrard KP, Barry JA, Muddiman DC. MSiReader: an open-source interface to view and analyze high resolving power MS imaging files on Matlab platform. Journal of the American Society for Mass Spectrometry 2013;24:718-721.
[20] Ghallab A, Myllys M, Friebel A, Duda J, Edlund K, Halilbasic E, et al. Spatio-Temporal Multiscale Analysis of Western Diet-Fed Mice Reveals a Translationally Relevant Sequence of Events during NAFLD Progression. Cells 2021;10:2516.
[21] **Godoy P, Hewitt NJ**, Albrecht U, Andersen ME, Ansari N, Bhattacharya S, et al. Recent advances in 2D and 3D in vitro systems using primary hepatocytes, alternative hepatocyte sources and non-parenchymal liver cells and their use in investigating mechanisms of hepatotoxicity, cell signaling and ADME. Archives of Toxicology 2013;87:1315-1530.
[22] Berg S, Kutra D, Kroeger T, Straehle CN, Kausler BX, Haubold C, et al. ilastik: interactive machine learning for (bio)image analysis. Nature Methods 2019;16:1226-1232.
[23] Friebel A, Johann T, Drasdo D, Hoehme S. Guided interactive image segmentation using machine learning and color based data set clustering. ArXiv 2020;abs/2005.07662.
[24] Bankhead P, Loughrey MB, Fernández JA, Dombrowski Y, McArt DG, Dunne PD, et al. QuPath: Open source software for digital pathology image analysis. Scientific Reports 2017;7:16878.
[25] Kluyver T, Ragan-Kelley B, Pérez F, Granger B, Bussonnier M, Frederic J, et al. Jupyter Notebooks – a publishing format for reproducible computational workflows. In: Loizides F, Scmidt B, editors. 20th International Conference on Electronic Publishing (01/01/16): IOS Press; 2016. p. 87-90.
[26] Yaniv Z, Lowekamp BC, Johnson HJ, Beare R. SimpleITK Image-Analysis Notebooks: a Collaborative Environment for Education and Reproducible Research. Journal of digital imaging 2018;31:290-303.
[27] van der Walt S, Schönberger JL, Nunez-Iglesias J, Boulogne F, Warner JD, Yager N, et al. scikit-image: image processing in Python. PeerJ 2014;2:e453.
[28] Bradski G. The OpenCV library. Dr Dobb's J Software Tools 2000;25:120-125.
[29] Fahlgren N, Feldman M, Gehan Malia A, Wilson Melinda S, Shyu C, Bryant Douglas W, et al. A Versatile Phenotyping System and Analytics Platform Reveals Diverse Temporal Responses to Water Availability in Setaria. Molecular Plant 2015;8:1520-1535.
[30] Schindelin J, Arganda-Carreras I, Frise E, Kaynig V, Longair M, Pietzsch T, et al. Fiji: an open-source platform for biological-image analysis. Nature Methods 2012;9:676-682.
[31] Thévenaz P, Ruttimann UE, Unser M. A pyramid approach to subpixel registration based on intensity. IEEE transactions on image processing : a publication of the IEEE Signal Processing Society 1998;7:27-41.
[32] Lee TC, Kashyap RL, Chu CN. Building Skeleton Models via 3-D Medial Surface Axis Thinning Algorithms. CVGIP: Graphical Models and Image Processing 1994;56:462-478.
[33] **Albrecht W, Kappenberg F, Brecklinghaus T**, Stoeber R, Marchan R, Zhang M, et al. Prediction of human drug-induced liver injury (DILI) in relation to oral doses and blood concentrations. Arch Toxicol 2019;93:1609-1637.
[34] Ritz C, Baty F, Streibig JC, Gerhard D. Dose-Response Analysis Using R. PloS one 2015;10:e0146021-e0146021.